TÜBİTAK

Turkish Journal of Earth Sciences

http://journals.tubitak.gov.tr/earth/

Research Article

Turkish J Earth Sci
(2016) 25: 418-433

doi:10.3906/yer-1510-5

Mineral chemistry of igneous rocks in the Lar Cu-Mo prospect, southeastern part of Iran: implications for P, T, and fO_2

Rahele MORADI[1,*], Mohammad BOOMERI[1], Sasan BAGHERI[1], Kazuo NAKASHIMA[2]

[1]Department of Geology, Faculty of Sciences, University of Sistan and Baluchestan, Zahedan, Iran

[2]Department of Earth and Environmental Sciences, Faculty of Science, Yamagata University, Yamagata, Japan

Received: 05.10.2015 • **Accepted/Published Online:** 07.06.2016 • **Final Version:** 24.10.2016

Abstract: The Lar Cu-Mo prospect is located 20 km north of Zahedan in Sistan and Baluchestan Province. This area is geologically situated in the Sistan Suture Zone. The Cu-Mo mineralization occurs as silicic veins in the Lar igneous rocks and includes hypogene chalcopyrite, bornite, and molybdenite mineralization. The syenite to monzonite host rocks occur as stock and dyke and display granular to porphyritic texture. In this study, mineral chemistry and petrographic examination of igneous rocks are used to constrain the crystallization conditions of the magma. The compositional range of plagioclase is relatively narrow (0.11%–26.05% An), whereas that of potassium feldspar is wide (11.80%–96.02% Or). Analyses of representative Lar biotite samples with electron microprobe analysis suggest that crystallization took place at average temperature of 731 °C. Amphiboles are calcic and compositionally range from pargasite to ferro-pargasite, edenite, actinolite, and magnesio-hornblende. Estimation of temperature and pressure using calcic amphibole geothermobarometry equations indicates that crystallization is estimated to have taken place at 831 °C and 7.65 kbar. Clinopyroxenes are mainly diopside and were crystallized in a magma chamber at an average temperature and pressure of 926 °C and 7.54 kbar, respectively. According to the mineral composition, the studied igneous rocks are calc-alkaline in magmatic series and were crystallized from a calc-alkaline oxidized magma. The whole-rock chemical data show that the study rocks are shoshonitic and high-K calc-alkaline.

Key words: Mineral chemistry, syenite, Cu-Mo mineralization, Lar, Sistan Suture Zone, southeastern part of Iran

1. Introduction

The Lar Cu-Mo prospect located 22 km north of Zahedan, southeast Iran, at the border with Pakistan and Afghanistan is proximal to Saindak and the giant Reko Diq copper deposits of Pakistan (Figure 1a). The Lar Cu-Mo prospect mainly occurs in syenitic to monzonitic igneous rocks of the Lar igneous complex (LIC). Although the LIC has been subject of several petrological and geochemical studies (Chance, 1981; Bagheri and Bakhshi, 2001; Nakisa, 2002; Karimi, 2002; Boomeri, 2004; Ghafari-Bijar, 2009; Farokh-Nezhad, 2011; Soltanian, 2013), the host rock characteristics of the Lar Cu-Mo prospect were the subject of few studies (Karimi, 2002; Nakisa, 2002; Dushangani, 2015). The Lar Cu-Mo prospect has been explored and drilled by the National Iranian Copper Industries Co. (Nakisa, 2002). The mineralization covers an area of 0.75 km^2 and contains several million tons of mineralized rocks averaging 0.2% Cu and 0.01% Mo (Nakisa, 2002; Dushangani, 2015). Although the mineralization is considered as a subeconomical mineralization (Dushangani, 2015), infill drilling to a nominal 250 m led to understand that the mineralization continues in deeper depths.

In general, the chemical compositions of minerals provide valuable information on the origin and nature and postsolidus modifications of the magmas, as well as the nature of the ore fluids associated with the magmas (Imai, 2000; Boomeri et al., 2009, 2010; Xianwu et al., 2009; Siahcheshm et al., 2012; Einali et al., 2014). Studying the chemistry of mineral assemblages and compositions of igneous rocks can assist in understanding the temperature, pressure, and fugacity ratios of a magma process (Idrus et al., 2007; Panigrahi et al., 2008; Einali et al., 2014).

Chemical compositions of rock-forming minerals in the Lar Cu-Mo prospect igneous rocks have not yet been determined. In this study, we present data on the mineral chemistry of primary minerals in igneous host rocks from the Lar Cu-Mo prospect. With data obtained from these minerals and by employing geothermobarometric methods, pressure, temperature, and oxygen fugacity

* Correspondence: rmoradi@pgs.usb.ac.ir

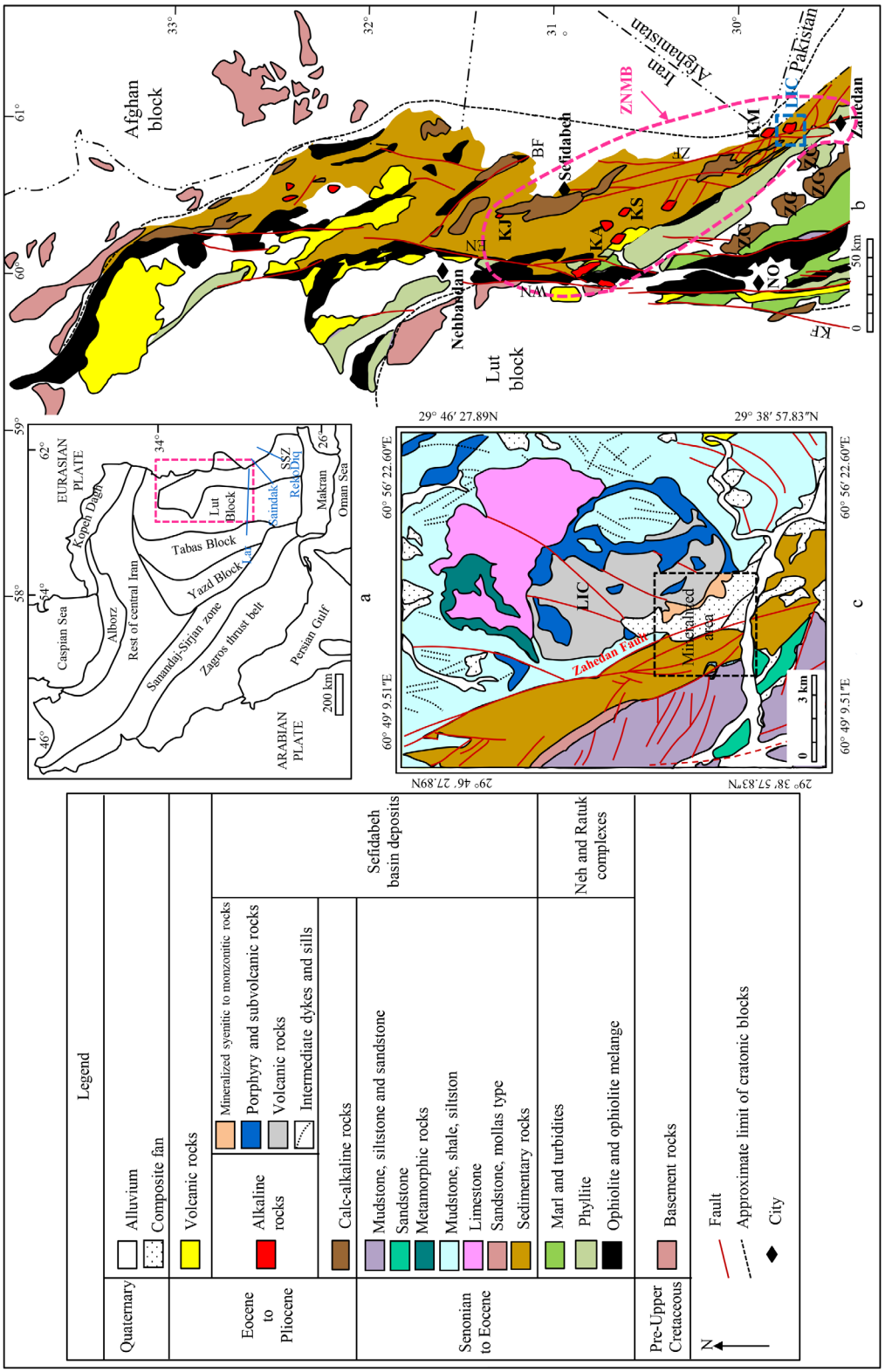

Figure 1. Geological maps of the a) main tectonostratigraphic units of Iran (Stöcklin, 1968), b) geological subdivisions of the SSZ and its principal igneous rock units (modified from Camp and Griffis, 1982; Tirrul et al., 1983). Faults are: BF, Bandan fault; EN, East Neh fault; WN, West Neh fault; ZF, Zahedan fault; KF, Kahurak Fault. Place names are: Sefidabeh (S), Nosratabad (NO). Intrusions are: Zahedan granites (ZG), Lar igneous complex (LIC), Kuh-e Malek Siah (KM), Kuh-e Seyasteragi (KS), Kuh-e Assagie (KA), Kuh-e Janja (KJ), Zahedan-Nehbandan magmatic belt (ZNMB). c) Geological maps of the Lar area (based on Behrouzi, 1993).

values were calculated. All these helped constrain the crystallization conditions and evolutions of the Lar Cu-Mo prospect.

2.Geology

The study area is located in the N–S trending 700-km-long Sistan Suture Zone (SSZ) (Figures 1a and b) that extends from Iran to Afghanistan and Pakistan. The SSZ is considered to have been a remnant of the late Cretaceous oceanic basin as a branch of the Neotethys. The SSZ was divided into the Neh-Ratuk accretionary prism and the Sefidabeh forearc basin (Figure 1b). Based on Camp and Griffis (1982) and Tirrul et al. (1983), the SSZ is characterized by the following features: A) the presence of Late Cretaceous ophiolites that are the oldest igneous rocks of this area and are the remnants of the Sistan oceanic crust between the Lut and Sistan blocks; B) flysch-type rocks that are the most dominant rocks in the SSZ and composed of Cretaceous to Paleocene sedimentary, metasedimentary, and siliceous clastic rocks; and C) nonophiolitic igneous rocks that are different in age, composition, and genesis and can be divided based on their age as follows: 1) Eocene calc-alkaline rocks of the accretionary prism that are related to subduction events in the area (Camp and Griffis, 1982); 2) Late Eocene Zahedan calc-alkaline I, rare S, and hybrid-type granitoids that are related to subduction and collision events in the area (Camp and Griffis, 1982; Sahebzadeh, 1996; Hosseini, 2002; Boomeri et al., 2005; Kord, 2005; Sadeghian, 2005; Sadeghian et al., 2005; Sadeghian and Valizadeh, 2007; Rahnama-Rad et al., 2008; Ghasemi et al., 2010; Moradi et al., 2014); 3) Oligocene to Middle Miocene alkaline and calc-alkaline igneous rocks of the Zahedan-Nehbandan narrow magmatic belt (ZNMB) (Camp and Griffis, 1982) (Figure 1b), where the alkaline magmatism is closely related to major transcurrent faults, which were important postcollisional structural features (Camp and Griffis, 1982); 4) Quaternary volcanic rocks like Mount Taftan that are related to the Makran active subduction of the Oman oceanic lithosphere under the Makran accretionary prism and the SSZ (Farhoudi and Karig, 1977). Although subduction, collision, and postcollisional events in the SSZ were confirmed by the majority of researchers, the mechanism and timing of the opening and closing of the oceanic basin has been differently discussed, i.e. subduction of the SSZ beneath the Afghan block (Camp and Griffis, 1982; Tirrul et al., 1983), subduction of the SSZ beneath the Lut block (Zarrinkoub et al., 2012), two-sided subduction of the SSZ beneath the Afghan and Lut blocks (Arjmandzadeh et al., 2011), and intraoceanic subduction by the east (Saccani et al., 2010).

The Lar Cu-Mo prospect in the west and southwest of the LIC is a part of the ZNMB at the southeastern extension of the SSZ (Figure 1b). The ZNMB is composed of alkaline, shoshonitic, and calc-alkaline extrusive and intrusive units where country rocks are represented by the flysch that accumulated in the accretionary prism setting. A number of igneous rocks were identified in the ZNMB such as the LIC and Malek Siah, Seyasteragi, and Janja intrusions and Assagie volcanic mountain. Pang et al. (2013) investigated igneous rocks in the north part of the ZNMB where magmatism was active from the middle Eocene (~46 Ma) to the late Oligocene (~25 Ma). The igneous rocks are calc-alkaline, high-K calc-alkaline (HKCA), and shoshonitic, triggered by convective removal of the lithosphere and resultant asthenospheric upwelling during postcollision extensional collapse of the SSZ in the Eocene-Oligocene (Pang et al., 2013).

The LIC is a late Oligocene elliptical (about 40 km^2 in size) igneous complex, hosted by flysch-type rocks of the Sefidabeh forearc (Figure 1c). Its bigger diameter is parallel to the Zahedan fault system in the western and southwestern parts. The main body of the LIC includes gray to dark-gray extrusive rocks such as lava and pyroclastic breccias, which were intruded by stocks, subvolcanic ring dykes, masses, and veins. The main igneous rocks of the LIC consist of trachyte, trachyandesite, andesite, tuff, volcanic breccia, hornblende-bearing porphyritic diorite, syenite, monzonite, latite, and calc-alkali to shoshonitic lamprophyres like minette, olivine minette, shonkinite, spessartite, and vogesite, which have been formed from shoshonitic and HKCA magmas (Chance, 1981; Bagheri and Bakhshi, 2001; Ghafari-Bijar, 2009; Farokh-Nezhad, 2011; Soltanian, 2013). Structurally, there are at least two main fault systems in the Lar Cu-Mo prospect with NW-SE and NE-SW trends (Karimi, 2002). The NW-SE system is mainly associated with mineralization and has been displaced by the younger NE-SW system.

3.Mineralization and alteration

The Lar Cu-Mo prospect is situated in the western and southwestern parts of the LIC (Figures 1a, 2a, 2b, and 3). The northeastern and eastern parts of the mineralized area consist of intermediate igneous rocks, and its southwestern and western parts consist of flysch type rocks (Figure 2a). The geology of the mineralized area consists of hornfels, shale, volcanic rocks, and syenitic to monzonitic igneous rocks. The flysch-type rocks such as siltstone and shale in the eastern side of the mineralized area are moderately to strongly recrystallized or metamorphosed to hornfels due to contact metamorphism effects of the Lar igneous rocks. The syenitic to monzonitic igneous rocks were also intruded by microsyenitic veins, quartz alkali feldspars syenite dykes, and silicic veins and veinlets (Figures 4a and b). Large blocks of the hornfels and metavolcanic rocks are common with syenitic to monzonitic igneous

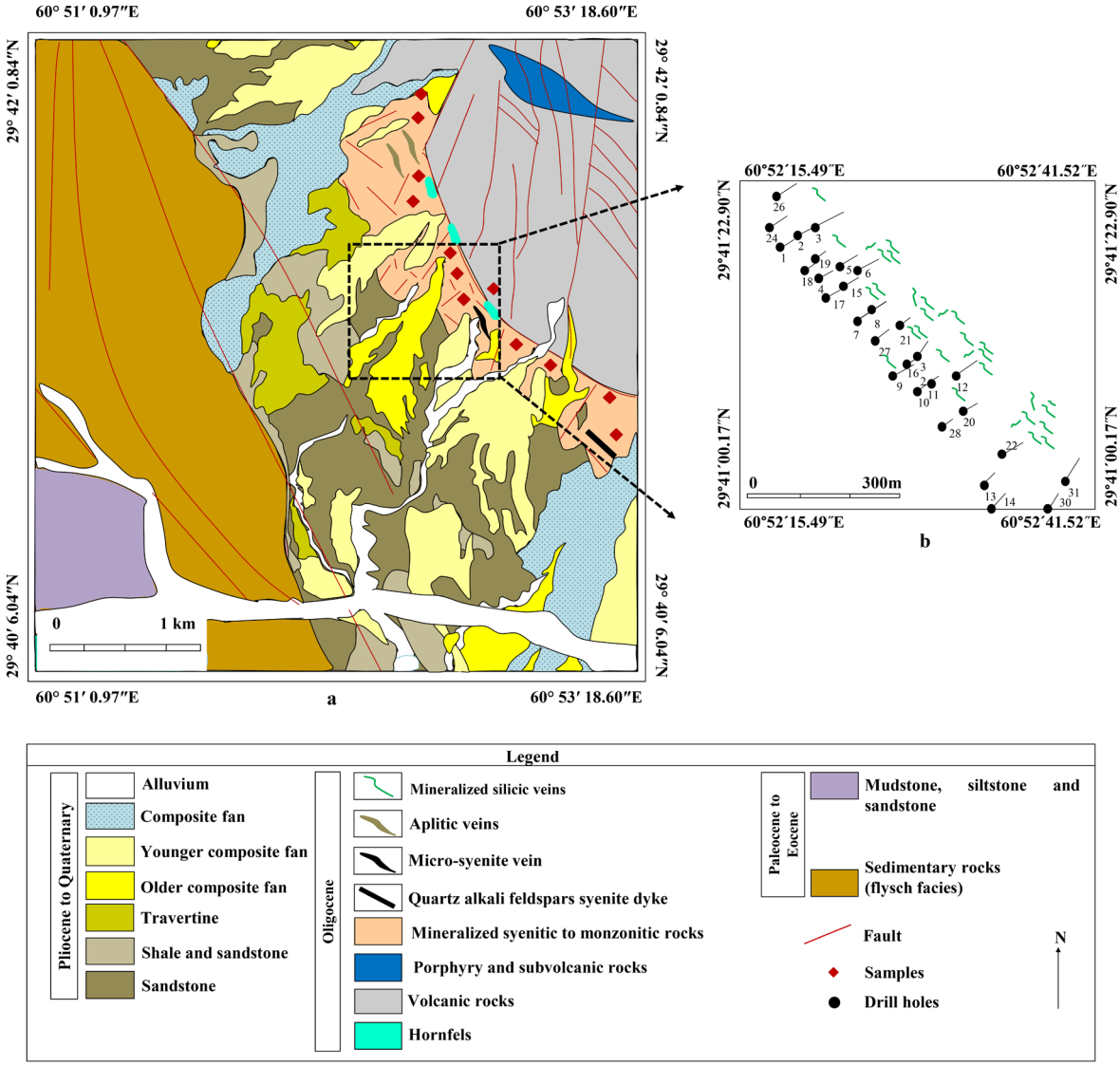

Figure 2. a) Geological map of the Lar Cu-Mo prospect (modified from Kan Iran Engineering, 1999), b) map location of bore holes with mineralized silicic veins in the Lar Cu-Mo prospect.

rocks, especially in the eastern side. The intrusive rocks that outcrop in the mineralized area are pinkish in color due to supergene alteration that obscures primary textures and mineralogy, especially in the upper levels. The Cu-Mo mineralization is primarily associated with silicic veins and veinlets (Figure 4c) that occur within syenite and monzonite and include chalcopyrite, bornite and molybdenite, magnetite, and hematite as well as supergene oxidation products of chalcocite, native copper, enargite, limonite, malachite, and azurite (Figures 4d–4f). Disseminated bornite and chalcopyrite only occur in the host rocks that are near the silicic veins and veinlets. The grades closely correlate with the density of the veins. Generally, the mineralized veins and veinlets show low density across the study area. Therefore, the host rocks mainly contain minor or no amounts of the mineralized silicic veins or veinlets.

The alteration zones in the study area are not regular and pervasive. They are often associated with tectonized locations, and they are more intense in the direction of the main faulted and fractured zones. Therefore, the fractures and faults play a significant role in the control of alteration and mineralization focus. As the main primary mineral of the host rocks is orthoclase, it is difficult to characterize the potassic alteration. This alteration type is characterized by the veins containing biotite and potassium feldspar associated with bornite, chalcopyrite, and/or molybdenite. It seems that some plagioclase was replaced by potassium

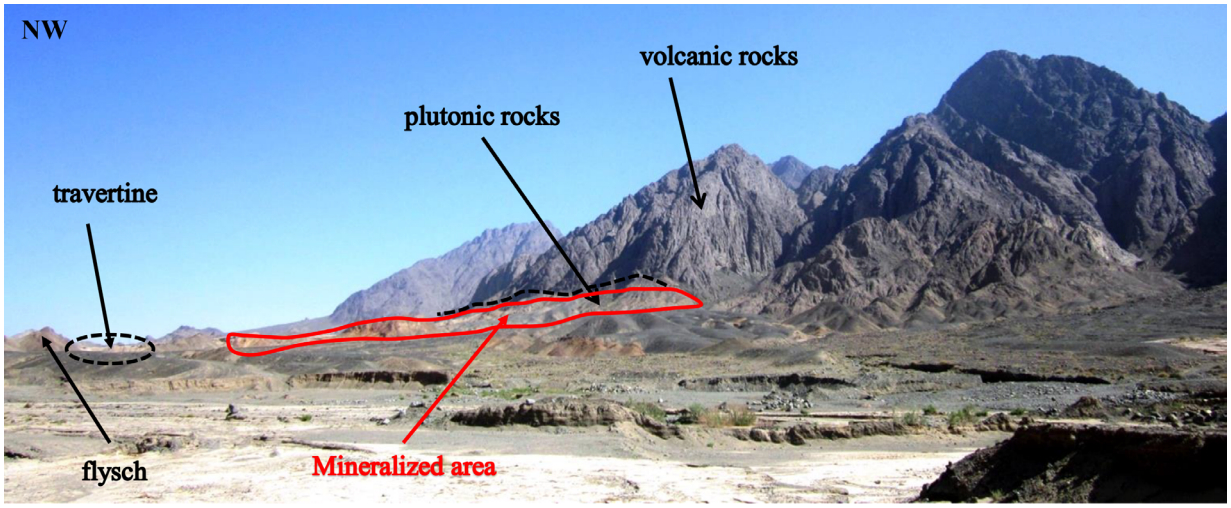

Figure 3. Field photograph of the Lar igneous complex and the Lar Cu-Mo mineralized area.

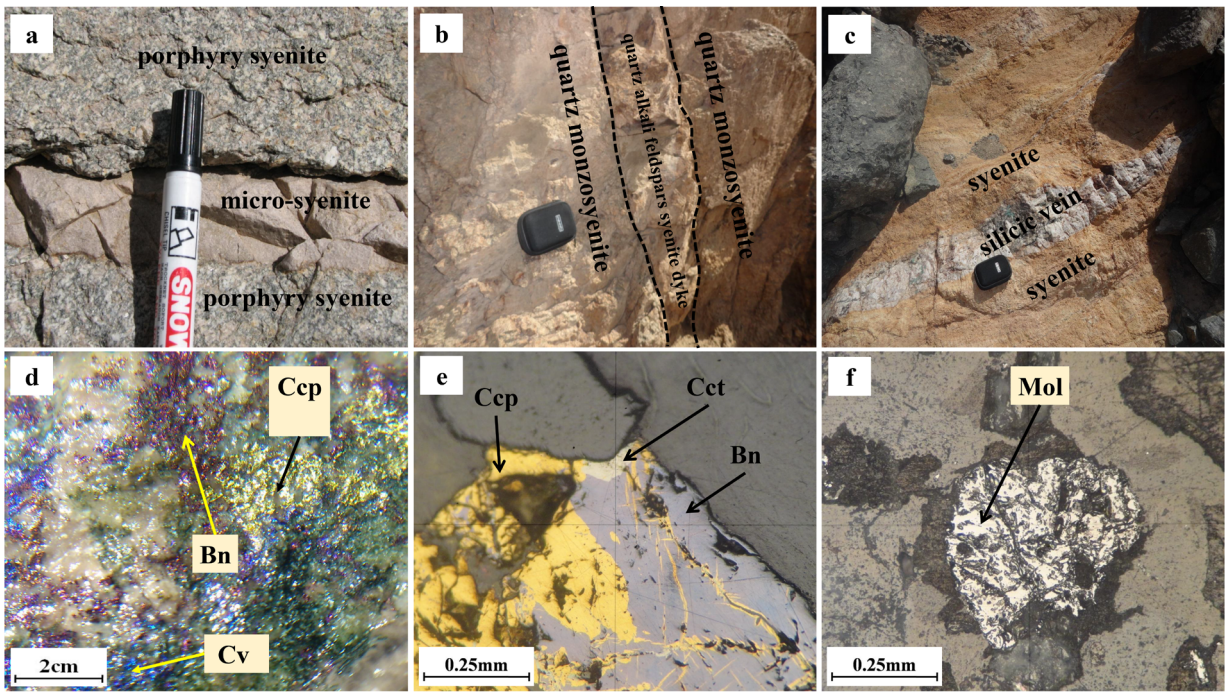

Figure 4. Field photographs of a) microsyenite vein in the porphyry syenite, b) quartz alkali feldspars syenite dyke, c) mineralized silicic vein, d) dispersed ore minerals in syenite. Photomicrographs of e) the same paragenesis of chalcocite, bornite, and chalcopyrite; f) molybdenite. Bn: Bornite, Cct: chalcocite, Ccp: chalcopyrite, Cv: covellite, Mol: molybdenite.

feldspar. Propylitic alteration is more widespread in peripheral parts of the mineralized area, especially in the hornfels and metavolcanic rocks. Epidote, calcite, chlorite, and minor sericite partially replaced magmatic pyroxene, hornblende, and biotite. Minor actinolite forms along the cleavage of the primary amphibole in a few samples. There are no distinct alteration zones of the phyllic and argillic in the studied parts of the mineralized area. However, the majority of the feldspars are partially replaced by sericite and clay minerals. Pyrite is a rare mineral in the mineralized area. The quartz veins and veinlets that are the most prominent character of the mineralized area may not be related to the phyllic alteration. Argillic alteration locally occurs in outcrops and shallow depths. This alteration type, which is characterized by clay minerals, iron hydroxide, and Cu carbonates, was probably formed by supergene processes.

4. Materials and methods

One hundred samples were collected from fresh and mineralized rocks from the surface and drill holes. The samples were examined by polarized microscope for petrographic and mineralographic descriptions at the University of Sistan and Baluchestan. Twelve thin-polished sections were chosen from less-altered syenitic to monzonitic igneous rocks with granular and porphyritic textures and tuff for electron microprobe analysis in order to determine their mineral composition.

In general, there are several generations of minerals in the Lar Cu-Mo prospect, but our analyzed minerals are magmatic feldspars, biotite, amphibole, and clinopyroxene. The selected magmatic minerals are commonly euhedral and subhedral in shape and show no evidence of having been replaced. Their modal percentages are based on visual estimates.

These minerals were analyzed by the automated JEOL JXA-8600 superprobe of Yamagata University with accelerating voltage of 15 kV, a beam current of 20 nA, a beam diameter of about 5 μm, detection limits of 0.05 wt. %, and a maximum 40-s counting interval. The diameter of the focused electron beam is about 5 μm. Data were processed by an online computer using the oxide ZAF in the XM-86 PAC program of JEOL. Calibration standards for the mentioned minerals were apatite, wollastonite, albite, adularia, synthetic SiO_2, TiO_2, Al_2O_3, Fe_2O_3, MnO, MgO, CaF_2, and NaCl. In each sample, several grains and several points of each mineral were analyzed based on textural relations, and an average of the analytical results was taken to represent the typical composition of that mineral in each sample. Formula calculations of feldspar, biotite, amphibole, and pyroxene are based on 32, 22, 23, and 6 atoms of oxygen, respectively. The amphiboles' ferric/ferrous ratios were calculated using 15-cation normalization and charge balance. The magmatic minerals in the granular syenitic rocks were used for employing geothermobarometric methods in order to determine crystallization conditions because these samples were not affected by weathering, overprinting, and late granodioritic veinlets.

5. Petrography

The dominant igneous rocks in the Lar Cu-Mo mineralized area are syenite and monzonite with lesser amounts of granodiorite and pyroclastic rocks. Syenite is dominantly medium- to coarse-grained, porphyritic, granular, and occasionally cataclastic in texture. There is extreme variation in the ratio of phenocrysts to groundmass. The groundmass ratio is less than 30% in porphyritic syenite and monzonite. The syenite is composed of plagioclase, clinopyroxene, and potassium feldspar as main minerals that crystallized at first and were followed by amphiboles, biotite, and Fe-Ti oxides. A second generation of feldspars and biotite can also be observed in some syenitic rock types. Moreover, sphene, apatite, zircon, and magnetite are common accessory minerals.

Orthoclase is the most abundant mineral in the syenite occurring as phenocrysts (Figure 5a) and groundmass. The orthoclase phenocrysts are euhedral to subhedral and up to 4 cm in size. Some of the phenocrysts of orthoclase poikilitically contain inclusions of biotite, titanite, apatite, pyroxene, and opaque minerals. The plagioclase is lath-shaped, euhedral to subhedral, and shows polysynthetic twinning (Figure 5b).

The biotite occurs as phenocryst (Figure 5c), tiny crystals in the groundmass, inclusions in the other minerals, and also secondary hydrothermal phases. Under the microscope, the biotite phenocrysts are mainly brown in color (in plane polarized light), variable in size, sometimes showing kink band twinning, with deformed cleavage, and have inclusions of apatite, titanite, and opaque minerals.

The amphibole occurs as phenocrysts and tiny crystals in shape, green in color (in plane polarized light), and variable in size (Figure 5d). Based on petrographic studies, the amphiboles mainly belong to the primary hornblende group and secondary actinolite. Clinopyroxene is the other ferromagnesian mineral in the Lar porphyry and granular syenitic rocks. Based on microscopic studies, greenish clinopyroxene occurs as subhedral to euhedral crystals in both phenocrysts (Figure 5e) and groundmass with variable size. The monzonite and syenite are petrographically similar and show extreme variation in the ratio of orthoclase to plagioclase. The monzonite has higher proportions of plagioclase relative to syenite.

The volcanic rocks occurred as lava and pyroclastic rocks. The volcanic rocks are mainly trachyte, latite, and andesite in composition, porphyritic and trachytic in texture, and gray and green in color. The phenocrysts are about 50% of these rocks and composed of plagioclase, potassium feldspar, amphiboles, biotite, and opaque mineral. The groundmass is composed of fine-grained crystals of feldspar and ferromagnesian minerals. Plagioclase and potassium feldspar are variable in size (up to 5 mm) and shape (euhedral to subhedral).

6. Mineral chemistry

6.1. Feldspar

Sixty-four points from six samples on feldspar phenocrysts of porphyritic igneous rocks and 31 points from three samples on granular igneous rocks were analyzed and plotted on the ternary orthoclase-albite-anorthite diagram of Deer et al. (1979) (Table 1; Figures 6 and 7). The potassium feldspars in the igneous rocks belong to sanidine-albite solid solutions in both porphyry and

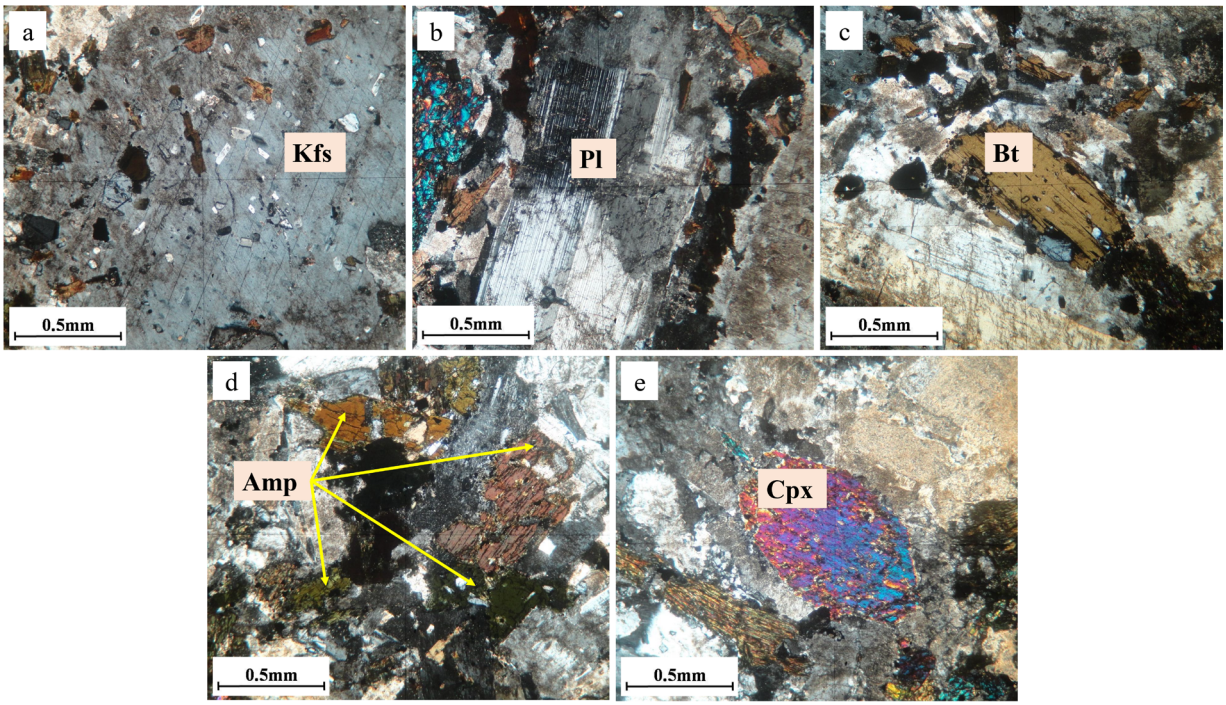

Figure 5. Cross-polarized light photomicrographs of a) alkali feldspars, b) plagioclase, c) biotite, d) amphibole, e) clinopyroxene. Kfs: Potassium feldspar, Pl: plagioclase, Bt: biotite, Amp: amphibole, Cpx: clinopyroxene.

granular igneous rocks (Figures 6 and 7). As petrographic studies show that the potassium feldspars are orthoclase, variation in Na contents is probably due to invisible cryptoperthite and microperthite in low-temperature feldspars (orthoclase and microcline) (MacKenzie and Smith, 1955). The plagioclases are mostly albite in both porphyry and granular rocks (Figures 6 and 7). Albite is the most common plagioclase in the syenitic rocks. Oligoclase and andesine belong to the late granodioritic phase that intruded on the syenite rocks.

6.2. Biotite

Twenty-four points from five samples and 15 points from three samples on biotite phenocrysts of porphyry and granular igneous rocks were analyzed, respectively (Table 2). The biotite compositions, when referred to the Al versus Fe/(Fe+Mg) (Rieder et al., 1998) diagram (Figure 8), clearly plot in the biotite field near the biotite and phlogopite line boundary. The biotites are the primary type (Figure 9), and they have a narrow range in chemical composition as SiO_2, Al_2O_3, TiO_2, and MgO range from 38.01 to 39.16, from 14.44 to 15.39, from 3.23 to 3.74, and from 14.74 to 15.50, respectively. It seems that the biotite is Mg- and Ti-rich and F- and Cl-poor.

6.3. Amphibole

Sixteen points from two samples and 14 points from one sample on amphibole phenocrysts of porphyry and granular igneous rocks were analyzed, respectively (Table 3). According to the classification of Leake et al. (1997), the associated amphibole phenocrysts with mineralized area are commonly calcic (pargasite to ferro-pargasite, edenite, actinolite, and magnesio-hornblende; Figure 10) with igneous nature (Figure 11).

In porphyry igneous rocks, amphiboles are chemically edenite, actinolite, and magnesio-hornblende with a high content of Mg and low content of Al and Ti. The actinolites are mainly due to weathering and alteration processes. According to Chivas (1981), amphiboles with Si of 7.3 (apfu) or less are generally considered magmatic and Si higher than 7.3 (apfu) is not a truly magmatic amphibole. The average content of Na_2O is higher than K_2O in amphiboles of both porphyry and granular igneous rocks. Moreover, based on Al content, the amphiboles can be also divided into two groups: low-Al amphiboles (actinolite, edenite, and magnesio-hornblende) and high-Al amphiboles (pargasite and ferro-pargasite) (Table 3).

6.4. Clinopyroxene

Four points from one sample on clinopyroxene phenocrysts of porphyritic igneous rocks and 14 points from two samples on granular igneous rocks were analyzed (Table 3). The representative Lar clinopyroxene analyses fall within the field of calcic composition. The clinopyroxenes have Al_2O_3 ranges from 2.58 to 3.25, and based on the classification of Deer et al. (1979), they are of the diopside type.

Table 1. Representative average chemical composition (wt. %) and structural formulae of feldspars in the Lar igneous rocks.

Rocks	Syenite												Monzonite			Tuff	
Textures	Porphyry						Granular						Porphyry			Porphyry	
Samples	L44		L18		L20		L79		L2		L90		L15		L30	L57	
Minerals	Pl	Afs	Pl	Afs	Pl	Afs	Pl	Afs	Pl	Afs	Pl	Afs	Pl	Afs	Pl	Pl	Afs
Number of grains	3	1	1	1	2	1	1	3	2	1	1	2	3	1	3	2	3
Number of points	7	2	7	4	7	3	1	12	5	3	4	6	11	3	8	4	8
	Av.	Av.	Av.	Av.	Av.	Av.	Av.	Av.	Av.	Av.	Av.	Av.	Av.	Av.	Av.	Av.	Av.
SiO_2 (wt. %)	73.79	68.45	63.22	70.36	73.77	70.87	69.66	69.75	72.45	68.92	71.22	67.18	72.34	71.47	74.22	67.08	65.79
TiO_2	0.02	0.00	0.02	0.01	0.01	0.04	0.00	0.02	0.02	0.01	0.02	0.02	0.01	0.02	0.01	0.02	0.04
Al_2O_3	20.86	18.89	24.51	19.10	20.93	19.53	21.32	19.44	21.38	19.94	21.74	21.22	21.39	19.56	20.74	21.08	20.50
FeO	0.15	0.86	0.46	0.07	0.07	0.12	0.02	0.09	0.16	0.12	0.07	0.18	0.13	0.05	0.05	0.18	0.59
MnO	0.00	0.00	0.01	0.01	0.00	0.00	0.00	0.01	0.02	0.01	0.02	0.01	0.01	0.01	0.01	0.00	0.02
MgO	0.01	0.00	0.01	0.00	0.03	0.00	0.01	0.00	0.05	0.00	0.01	0.13	0.02	0.00	0.00	0.01	0.04
CaO	0.54	0.04	6.05	0.02	0.55	0.36	1.79	0.31	0.56	0.57	1.99	0.21	1.54	0.05	0.47	6.50	0.10
Na_2O	7.07	0.91	6.46	0.35	6.22	2.45	7.36	2.27	5.84	1.98	7.23	1.53	6.63	0.35	7.13	5.90	1.47
K_2O	0.36	13.61	0.32	13.09	0.60	9.91	0.20	10.87	1.25	11.49	0.82	12.53	0.71	12.63	0.11	0.15	13.13
BaO	0.02	0.11	0.04	0.20	0.02	0.37	0.03	0.26	0.05	0.14	0.02	0.08	0.05	0.18	0.03	0.01	0.63
Total	102.82	102.87	101.10	103.21	102.20	103.65	100.39	103.01	101.78	103.17	103.14	103.10	102.83	104.31	102.78	100.93	102.30
Numbers of cations on the basis of 32 O																	
Si (apfu)	12.280	12.127	11.046	12.280	12.317	12.225	11.970	12.167	12.202	12.047	11.954	11.815	12.108	12.293	12.328	11.641	11.804
Ti	0.003	0.000	0.003	0.001	0.001	0.005	0.000	0.003	0.003	0.001	0.003	0.003	0.001	0.003	0.001	0.003	0.005
Al	4.091	3.944	5.047	3.930	4.118	3.970	4.318	3.996	4.243	4.108	4.300	4.398	4.219	3.965	4.060	4.311	4.335
Fe^{2+}	0.021	0.127	0.067	0.010	0.010	0.017	0.003	0.013	0.023	0.018	0.010	0.026	0.018	0.007	0.007	0.026	0.089
Mn	0.000	0.000	0.001	0.001	0.000	0.000	0.000	0.001	0.003	0.001	0.003	0.001	0.001	0.001	0.001	0.000	0.003
Mg	0.002	0.000	0.003	0.000	0.007	0.000	0.003	0.000	0.013	0.000	0.003	0.034	0.005	0.000	0.000	0.003	0.011
Ca	0.096	0.008	1.132	0.004	0.098	0.067	0.330	0.058	0.101	0.107	0.358	0.040	0.276	0.009	0.084	1.208	0.019
Na	2.281	0.313	2.188	0.118	2.013	0.819	2.452	0.768	1.907	0.671	2.353	0.522	2.151	0.117	2.296	1.985	0.511
K	0.076	3.076	0.071	2.915	0.128	2.181	0.044	2.419	0.269	2.562	0.176	2.811	0.152	2.771	0.023	0.033	3.005
Ba	0.001	0.008	0.003	0.014	0.001	0.025	0.002	0.018	0.003	0.010	0.001	0.006	0.003	0.012	0.002	0.001	0.044
Total	18.852	19.602	19.561	19.279	18.695	19.309	19.121	19.443	18.765	19.524	19.159	19.655	18.936	19.178	18.802	19.211	19.826
An (mol %)	3.92	0.22	33.39	0.12	4.39	2.17	11.66	1.77	4.44	3.18	12.40	1.17	10.71	0.32	3.48	37.45	0.52
Ab	92.96	9.20	64.51	3.90	89.90	26.72	86.78	23.68	83.76	20.07	81.52	15.49	83.42	3.99	95.52	61.52	14.43
Or	3.11	90.57	2.10	95.98	5.71	71.11	1.55	74.54	11.80	76.74	6.08	83.33	5.88	95.69	1.00	1.03	85.04

Afs: Potassium feldspars, Pl: plagioclase, An: anorthite, Ab: albite, Or: orthoclase.

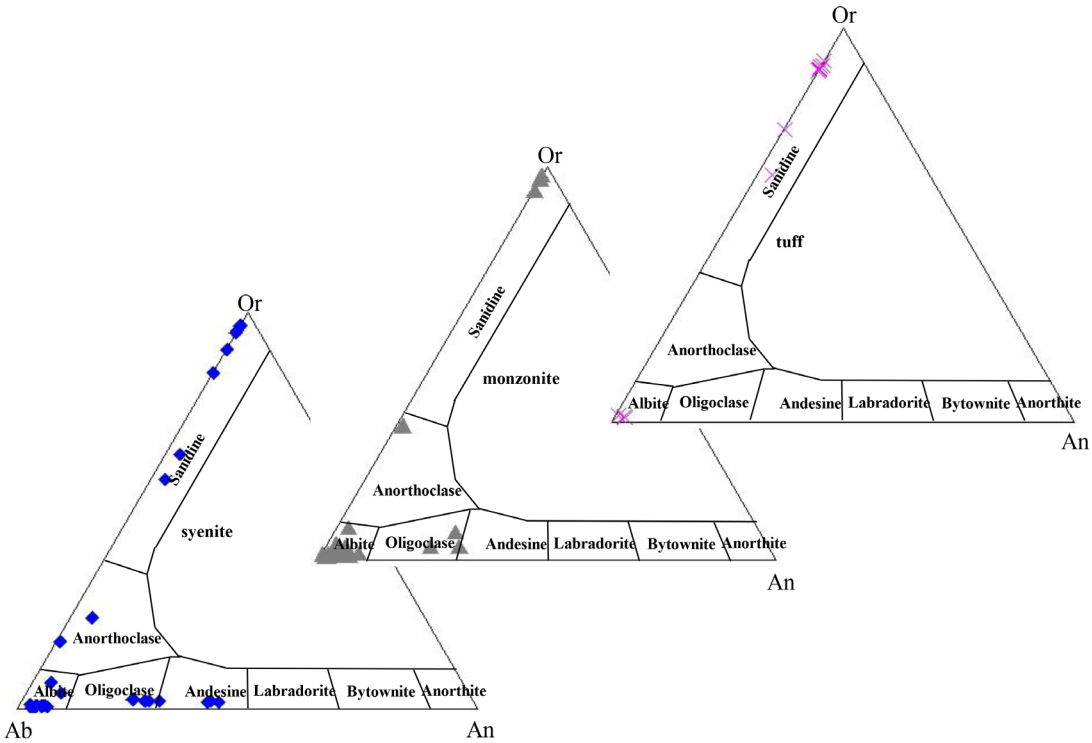

Figure 6. Classification of feldspars in the Lar Cu-Mo prospect porphyry igneous rocks on a ternary orthoclase-albite-anorthite diagram. Field boundaries from Deer et al. (1979).

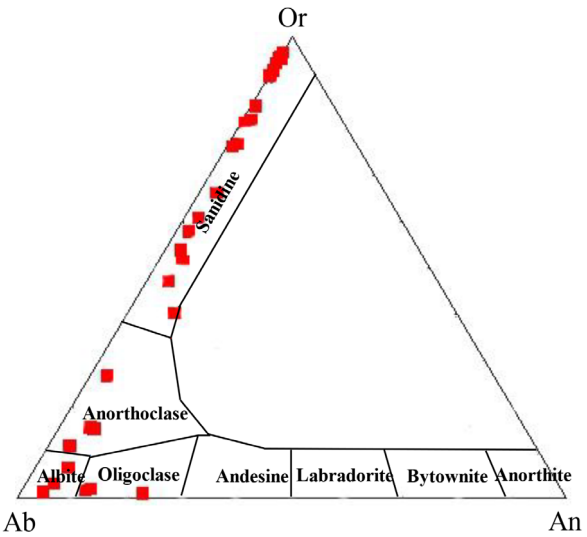

Figure 7. Classification of feldspars in the Lar Cu-Mo prospect granular igneous rocks on a ternary orthoclase-albite-anorthite diagram. Field boundaries from Deer et al. (1979).

7. Crystallization conditions

7.1. Temperature

The concentration of Ti and the Ti/ Fe^{2+} ratio in biotite are very sensitive to temperature, making it possible to use biotite to obtain reliable temperature estimates in igneous and metamorphic rocks (Luhr et al., 1984; Patino Douce, 1993). We used the empirical Ti/ Fe^{2+} geothermometer of Luhr et al. (1984) to calculate plutonic biotite precipitation temperatures in the granular igneous rocks with the following equation:

$$T(^{\circ}\mathrm{K}) = \frac{838}{(1.0337 - \frac{\mathrm{Ti}}{\mathrm{Fe}^{2+}})}$$

Calculated temperatures for biotite from granular syenitic rocks show an average temperature of 731 °C.

Amphibole thermometry for pargasites and ferro-pargasites in the Lar granular syenitic rocks was calibrated according to the method of Ridolfi et al. (2010) with the following equation:

$$T(^{\circ}\mathrm{C}) = -151.487 * \mathrm{Si}^{*} + 2.041$$

where

$$\mathrm{Si}^{*} = \mathrm{Si} + \frac{^{[4]}\mathrm{Al}}{15} + 2\,^{[4]}\mathrm{Ti} - \frac{^{[6]}\mathrm{Al}}{2} - \frac{^{[6]}\mathrm{Ti}}{1.8} + \frac{\mathrm{Fe}^{3+}}{9} + \frac{\mathrm{Fe}^{2+}}{3.3} + \frac{\mathrm{Mg}}{26} + \frac{^{B}\mathrm{Ca}}{5} + \frac{^{B}\mathrm{Na}}{1.3} - \frac{^{A}\mathrm{Na}}{15} + \frac{^{A}\square}{2.3}$$

The calculations suggest a mean temperature of 831 °C.

The electron microprobe analyses of pyroxene can also be used in thermometry based on the method of

Table 2. Representative average chemical composition (wt. %) and structural formulae of biotite in the Lar igneous rocks.

Rocks	Syenite					Monzonite		Tuff
Textures	Porphyry		Granular			Porphyry		Porphyry
Samples	L18	L20	L2	L12	L3	L15	L13	L57
Number of grains	2	1	1	2	2	1	2	2
Number of points	6	2	3	6	6	3	6	7
	Av.	Av.	Av.	Av.	Av.	Av.	Av.	Av.
SiO2 (wt. %)	38.27	38.35	38.94	39.00	38.01	39.16	39.14	38.95
TiO2	3.55	3.68	3.70	3.48	3.66	3.44	3.44	3.23
Al2O3	15.16	14.70	15.09	14.44	15.30	14.51	14.73	15.39
FeO	16.41	16.88	15.96	16.07	16.87	16.83	15.86	16.05
MnO	0.20	0.21	0.28	0.24	0.26	0.20	0.31	0.24
MgO	15.10	14.95	14.94	15.33	14.75	14.74	15.14	15.58
CaO	0.03	0.05	0.03	0.05	0.03	0.14	0.07	0.04
Na2O	0.12	0.14	0.15	0.12	0.18	0.11	0.13	0.23
K_2O	9.14	8.16	9.30	8.88	9.33	8.65	8.92	8.55
BaO	0.08	0.26	0.10	0.12	0.10	0.10	0.16	0.22
Cl	0.09	0.08	0.06	0.13	0.07	0.13	0.08	0.03
F	0.31	0.21	0.28	0.23	0.22	0.39	0.41	0.23
Total	98.46	97.67	98.89	98.12	98.79	98.4	98.39	98.74
Numbers of cations on the basis of 22 O								
Si (apfu)	5.551	5.598	5.610	5.657	5.519	5.671	5.655	5.600
^{IV}Al	2.449	2.402	2.390	2.343	2.481	2.329	2.345	2.400
T Site	8.000	8.000	8.000	8.000	8.000	8.000	8.000	8.000
^{VI}Al	0.144	0.128	0.173	0.127	0.138	0.149	0.164	0.209
Ti	0.387	0.404	0.401	0.380	0.400	0.375	0.374	0.349
Fe	1.991	2.061	1.923	1.950	2.049	2.038	1.916	1.930
Mn	0.025	0.026	0.034	0.029	0.032	0.025	0.038	0.029
Mg	3.264	3.253	3.208	3.314	3.192	3.181	3.260	3.338
O site	5.811	5.872	5.745	5.803	5.812	5.768	5.753	5.856
Ca	0.005	0.008	0.005	0.008	0.005	0.022	0.011	0.006
Na	0.034	0.040	0.042	0.034	0.051	0.031	0.036	0.064
K	1.691	1.520	1.709	1.643	1.728	1.598	1.644	1.568
Ba	0.005	0.015	0.006	0.007	0.006	0.006	0.009	0.012
A site	1.730	1.567	1.756	1.685	1.784	1.651	1.692	1.639
Cl	0.011	0.010	0.007	0.016	0.009	0.016	0.010	0.004
F	0.071	0.048	0.064	0.053	0.051	0.089	0.094	0.052
OH	3.918	3.942	3.929	3.931	3.941	3.895	3.897	3.944
X_{Mg}	0.621	0.612	0.625	0.630	0.609	0.610	0.630	0.634
T °C			742	726	726			

OH is calculated by OH = 4 – (Cl + F); X_{Mg} = Mg / (Mg + Fe).

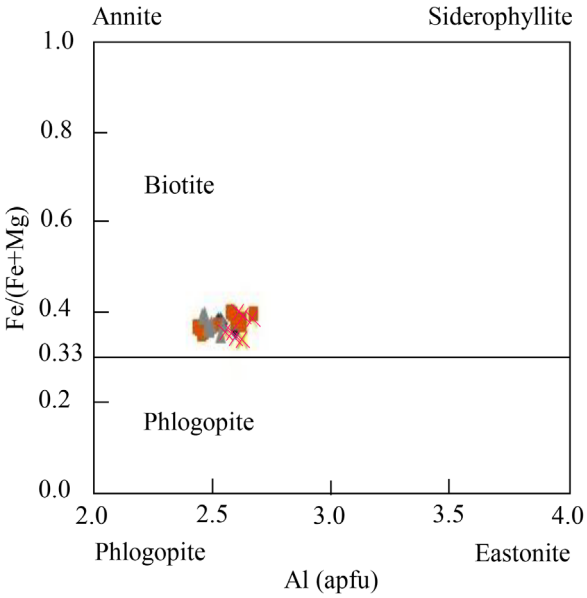

Figure 8. Plot of Fe / (Fe + Mg) versus ΣAl showing the classification of biotite. Field boundaries from Rieder et al. (1998). Similar symbols as in Figures 6 and 7.

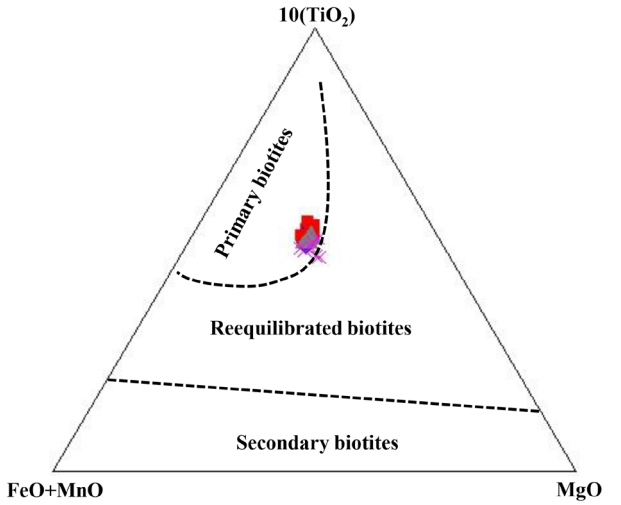

Figure 9. Chemical composition of biotite crystals using the (FeO + MnO) – $10TiO_2$ – MgO ternary diagram (Nachit et al., 2005). Similar symbols as in Figures 6 and 7.

Dal Negro et al. (1982). They calculated the temperature of crystallization for pyroxenes based on the following equation:

$$T(^{o}\mathrm{K}) = \left[1000\ \frac{5.465(R^{3+}) + 7.324Ca^{"} - 3.039}{-\ln K_D + 4.032(R^{3+}) + 5.383Ca^{"} - 3.767}\right]$$

Here,

$Ca^{"} = (Ca + Na + Mn)$,

$R^{3+} = (Al^{VI} + Fe^{3+} + Cr + Ti^{4+})$,

and $K_D = \frac{Mg}{(Mg + Fe^{2+})^{Cpx}}$

Depending on this calculation, the clinopyroxene average temperature from the granular syenitic rocks is 926 °C.

7.2. Pressure

The barometric method of Nimis (1999) was used for pyroxene barometry with following equation:

$$P\ (\pm 1.10\ kbar) = 621.151 - 1.220V_{Cell}^{P,T} - 4.620V_{M1}^{P,T} - 7.773mg$$

Here, $mg = \frac{Mg}{(Mg + Fe^{2+})^{Cpx}}$ and $V_{Cell}^{P,T}$ and $V_{M1}^{P,T}$ show volumes corrected for thermal expansivity and compressibility at valid P-T conditions. Based on this equation, the calculated average pressure of clinopyroxene from the granular syenitic rocks is 7.54 kbar.

On the other hand, geobarometric estimates for granular syenitic rocks could be attempted based on Al total content in amphibole following the method of Ridolfi et al. (2010):

$$P(\mathrm{MPa}) = 19.209e^{(1.438\mathrm{Al_{Tot}})}$$

The estimated pressure for pargasite and ferro-pargasite crystallization in the studied granular syenitic rocks is about 7.65 kbar (R^2 = 0.99). Although Al_2O_3 contents of the Lar pargasites and ferro-pargasites are high and we can ascribe this to their crystallization at higher pressures, in general Al in amphiboles increases with both P and T, and compositional variations (high proportions of melt) also seem to influence the partitioning of Al_2O_3 in Ca-amphibole (Ali, 2012). Since the parental magma of the Lar Cu-Mo prospect igneous rocks is shoshonitic in nature and high Al contents are one of the main characters of this kind of magma, the high Al contents in the studied amphiboles depend on Al contents in the melt.

7.3. Oxygen fugacity (fO_2)

Ridolfi et al. (2010) proposed an empirical universal amphibole sensor to estimate fO_2 parameters with the following equation:

$$\Delta NNO = 1.644\ Mg^{*} - 4.01$$

where

$$Mg^{*} = Mg + \frac{Si}{47} - \frac{^{[6]}Al}{9} - 1.3^{[6]}Ti + \frac{Fe^{3+}}{3.7} + \frac{Fe^{2+}}{5.2} - \frac{^{B}Ca}{20} - \frac{^{A}Na}{2.8} + \frac{^{A}\square}{9.5}$$

Table 3. Representative average chemical composition (wt. %) and structural formulae of pyroxene and amphiboles in the Lar igneous rocks.

Rocks	Syenite			Rocks	Syenite		
Minerals	Amphibole			Minerals	Clinopyroxene		
Textures	Porphyry		Granular	Textures	Porphyry	Granular	
Samples	L44	L20	L2	Samples	L18	L2	L3
Number of grains	1	3	1	Number of grains	1	1	3
Number of points	2	14	10	Number of points	4	4	10
	Av.	Av.	Av.		Av.	Av.	Av.
SiO2 (wt. %)	55.00	54.51	40.79	SiO2 (wt. %)	52.62	51.81	52.74
TiO2	0.25	0.39	2.09	TiO2	0.35	0.43	0.37
Al2O3	1.88	2.32	12.62	Al2O3	2.58	3.25	2.67
FeO	8.97	9.82	17.69	FeO	7.41	7.42	8.06
MnO	0.26	0.33	0.42	MnO	0.40	0.30	0.34
MgO	18.75	17.31	9.99	MgO	13.78	13.29	13.29
CaO	12.55	13.52	11.44	CaO	22.61	21.84	22.88
Na2O	0.75	0.80	2.22	Na2O	0.96	1.11	1.05
K_2O	0.22	0.20	1.90	K_2O	0.01	0.06	0.01
Total	98.41	99.00	97.26	Total	100.72	99.51	101.41
Numbers of cations on the basis of 23 O				Numbers of cations on the basis of 6 O			
Si (apfu)	7.728	7.673	6.144	Si (apfu)	1.942	1.933	1.940
$Al^{(iv)}$	0.272	0.327	1.856	$Al^{(iv)}$	0.058	0.067	0.060
T Site	8.000	8.000	8.000	T site	2.000	2.000	2.000
$Al^{(vi)}$	0.040	0.058	0.384	$Al^{(vi)}$	0.054	0.076	0.055
Fe^{3+}	0.000	0.000	0.000	Ti	0.010	0.012	0.010
Ti	0.026	0.041	0.237	Mg	0.694	0.671	0.676
Fe^{2+}	1.054	1.156	2.228	Fe^{2+}	0.229	0.232	0.248
Mn	0.031	0.039	0.054	Mn	0.013	0.009	0.011
Mg	3.928	3.633	2.243	M1 site	1.000	1.00	1.000
Ca	1.889	2.039	1.846	Mg	0.064	0.068	0.053
C + B site	6.968	6.966	6.992	Ca	0.894	0.873	0.902
Na	0.204	0.218	0.648	Na	0.069	0.080	0.075
K	0.039	0.036	0.365	K	0.000	0.003	0.000
A site	0.244	0.254	1.013	M2 site	1.027	1.024	1.030
X_{Mg}	0.788	0.759	0.502	X_{Mg}	0.768	0.761	0.746
T (°C)	-	-	831	T (°C)	-	924	928
P (kbar)	-	-	7.65	P (kbar)	-	6.84	8.23

X_{Mg} = Mg / Mg + Fe

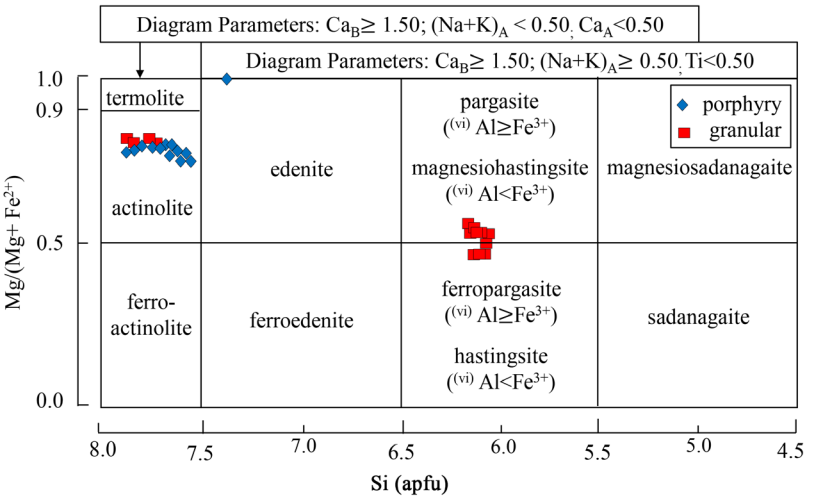

Figure 10. Plot of microprobe analyses showing the compositional range of the amphiboles. Field boundaries from Leake et al. (1997). Similar symbols as in Figures 6 and 7.

According to this equation, the value of log fO_2 calculated for granular syenitic rocks is –11.1 (maximum error: 0.41 log units).

7.4. Nature of the magma and geotectonic environment

Mineral chemistry can be used to discriminate magmatic series and the tectonic environment of igneous rocks (e.g., Le Bas, 1962; Leterrier et al., 1982; Nachit, 1986; Abdel-Rahman, 1994; Molina et al., 2009). According to the biotite, amphibole, and pyroxene discrimination diagrams of Abdel-Rahman (1994), Molina et al. (2009), and Le Bas (1962) respectively, the biotite, amphibole, and pyroxene from the Lar Cu-Mo prospect igneous rocks plot in the calc-alkaline fields (Figure 12). The diagrams based on the mineral chemistry do not discriminate the calc-alkaline, HKCA, and shoshonitic magmatic series. According to Bagheri and Bakhshi (2001), the Lar igneous rocks are HKCA and shoshonitic in magmatic series, which is real nature of the studied rocks.

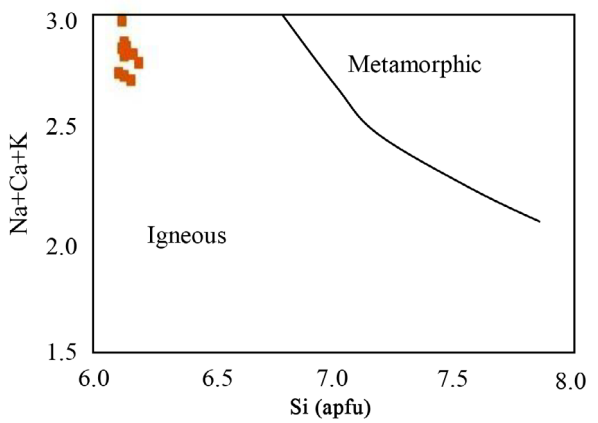

Figure 11. Plot of Si versus Na + Ca + K to discriminate igneous and metamorphic amphiboles (Sial et al., 1998). Similar symbols as in Figure 7.

Although the main magmatism in the Lar area is HKCA and shoshonitic and this kind of magma can occur in a subduction setting (Müller and Groves, 1997), the determined age of the LIC using the K/Ar isotopic system on biotite and whole rock yields ages ranging from 27.8 to 32 Ma (Camp and Griffis, 1982), younger than the collision time (33 Ma) of Sistan and Lut blocks in the southeastern part of Iran, indicating a postcollisional tectonic setting for the Lar magmatism. Generally, K-rich magmatism in postcollisional tectonic settings is associated with strike-slip faults. The strike-slip faults are able to channel mantle material and indirectly provide heat that can induce melting of lithospheric material and create a space for magmas that mantle melts injected beneath strike-slip faults, as a result of decompression melting (Pirajno, 2010). This is in compliance with the location of the LIC that was formed in the southern side of the Zahedan strike-slip fault system.

8. Summary and conclusion

Based on the field studies of the rock units in the Lar Cu-Mo prospect, from older to younger are hornfels, lava and pyroclastic rocks, syenitic to monzonitic stocks, aplitic veins, the late granodioritic phase, and nonmineralized and mineralized silicic veins, respectively. Moreover, petrographic studies show that potassium feldspar, plagioclase, and clinopyroxene crystallized first, followed by amphiboles, biotite, and Fe-Ti oxides, which may be surrounded by narrow rims of ilmenite that may additionally occur as discrete, subhedral to anhedral grains together with a second generation of feldspars.

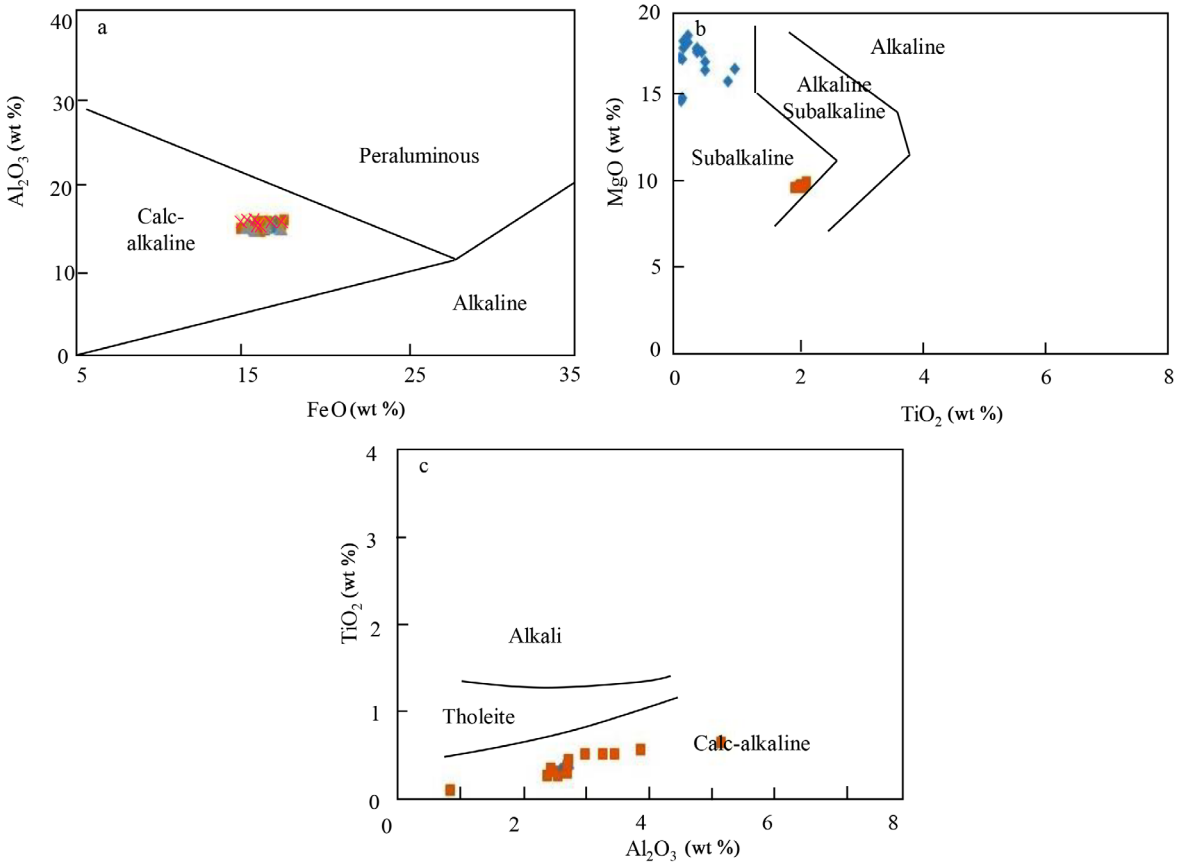

Figure 12. Composition of biotite, amphibole, and pyroxene in the discrimination magmatic affinity diagrams of a) Abdel-Rahman (1994), b) Molina et al. (2009), and c) Le Bas (1962). Similar symbols as in Figures 6 and 7.

The mineral chemistry analyses indicate that the Lar prospect clinopyroxenes are mainly diopside in composition and they were crystallized in a magma chamber at a temperature and pressure from 926 °C and 7.54 kbar, respectively. Moreover, all of the amphiboles in the mineralized area are calcic. In contrast to the barren igneous rock amphiboles in the Lar area that are edenite in composition (Farokh-Nezhad, 2011), the amphiboles in the mineralized area are pargasite to ferro-pargasite, edenite, actinolite, and magnesio-hornblende and this is an important criterion for distinguishing mineralized igneous rocks from the barren type. The representative Lar biotite analyses fall within the field of biotite composition that crystallized at 731 °C. It seems that this is the lowest emplacement temperature of the Lar igneous rocks. The mineral composition of the Lar Cu-Mo mineralization is consistent with crystallization from calc-alkaline oxidized magma.

References

Abdel-Rahman AM (1994). Nature of biotites from alkaline, calc-alkaline and peraluminous magmas. J Petrol 35: 525-541.

Ali SA (2012). Geochemistry and geochronology of Tethyan-arc related igneous rocks, NE Iraq. PhD, University of Wollongong, Wollongong, Australia.

Arjmandzadeh R, Karimpour MH, Mazaheri SA, Santos JF, Medina JM, Homam SM (2011). Sr\Nd isotope geochemistry and petrogenesis of the Chah-Shaljami granitoids (Lut Block, Eastern Iran). J Asian Earth Sci 41: 283-296.

Bagheri S, Bakhshi MR (2001). Investigation of North Zahedan Magmatism and Its Relation to Ore Genesis. Zahedan, Iran: University of Sistan and Baluchestan.

Behrouzi A (1993). Geological Map of Zahedan Quadrangle (1:250000). Tehran, Iran: Geological Survey of Iran.

Boomeri M (2004). Mineralogy and geochemistry of Lar mountains igneous rocks in northern part of Zahedan. In: 12th Symposium of Crystallography and Mineralogy of Iran.

Boomeri M, Lashkaripour GR, Gorgij MN (2005). F and Cl in biotites from Zahedan granitic rocks. Iranian Journal of Crystallography and Mineralogy 13: 79-94.

Boomeri M, Nakashima K, Lentz DR (2009). The Miduk porphyry Cu deposit, Kerman, Iran: a geochemical analysis of the potassic zone including halogen element systematics related to Cu mineralization processes. J Geochem Explor 103: 17-29.

Boomeri M, Nakashima K, Lentz DR (2010). The Sarcheshmeh porphyry copper deposit, Kerman, Iran: a mineralogical analysis of the igneous rocks and alteration zones including halogen element systematic related to Cu mineralization processes. Ore Geol Rev 38: 367-381.

Camp VE, Griffis RJ (1982). Character, genesis and tectonic setting of igneous rocks in the Sistan Suture Zone, eastern Iran. Lithos 15: 221-239.

Chance P (1981). Petrogenesis of a low-Ti, potassic suite: Kuh-e Lar caldera subsidence complex, eastern Iran. MSc, University of Western Ontario, London, Canada.

Chivas AR (1981). Geochemical evidence for magmatic fluids in porphyry copper mineralization, part 1: Mafic silicates from the Koloula igneous complex. Contrib Mineral Petrol 78: 289-403.

Dal Negro A, Carbonin S, Molin GM, Cundari A, Piccirillo EM (1982). Intracrystalline cation distribution in natural clinopyroxenes of tholeiitic, transitional, and alkaline basaltic rocks. In Saxena SK, editor. Advances in Physical Geochemistry. Vol. 2. Berlin, Germany: Springer, pp. 117-150.

Deer WA, Howie RA, Zussman J (1979). An Introduction to the Rock Forming Minerals. London, UK: Longman.

Dushangani F (2015). Mineralogy, alteration and origin of cu mineralization in Lar, north of Zahedan, east of Iran[' . MSc, University of Sistan and Baluchestan, Zahedan, Iran.

Einali M, Alirezaei S, Federica A (2014). Chemistry of magmatic and alteration minerals in the Chahfiruzeh porphyry copper deposit, south Iran: implications for the evolution of the magmas and physicochemical conditions of the ore fluids. Turkish J Earth Sci 23: 147-165.

Farhoudi G, Karig DE (1977). Makran of Iran and Pakistan as an active arc system. J Geol 5: 664-668.

Farokh-Nezhad M (2011). Geochemical characterization of potassic mafic rocks, monzonites and syenites from Lar complex, eastern Iran, MSc, University of Sistan and Baluchestan, Zahedan, Iran.

Ghafari-Bijar S (2009). Geochemistry of potassic mafic rocks in the Lar complex, north of Zahedan, east of Iran. MSc, University of Sistan and Baluchestan, Zahedan, Iran.

Ghasemi H, Sadeghian M, Kord M, Khanalizadeh A (2010). The evolution mechanisms of Zahedan granitoidic batholith, southeast Iran. Iranian Journal of Crystallography and Mineralogy 17: 551-578.

Hosseini MR (2002). Petrology and geochemistry of SW-Zahedan granitoids. MSc, University of Tehran, Tehran, Iran.

Idrus A, Kolb J, Meyer FM (2007). Chemical composition of rock forming minerals in copper-gold-bearing tonalite porphyries at the Batu Hijau deposit, Sumbawa Island, Indonesia: implications for crystallization conditions and fluorine-chlorine fugacity. Resour Geol 57: 102-113.

Imai A (2000). Genesis of the Mamut porphyry Cu deposit, Sabah, east of Malaysia. Resour Geol 50: 1-23.

Kan Iran Engineering (1999). Report of the Lar Copper Deposit Geological Map. Tehran, Iran: National Iranian Copper Industries Co.

Karimi A (2002). Geochemical behaviors and geological studies of copper and paragenesis elements in Lar mineralization (North Zahedan). Geosciences Scientific Quarterly Journal 43: 56-67.

Kord M (2005). Petrology and geochemistry of Cheshme Bid granitoids, southeast of Zahedan. MSc, Shahrood University of Technology, Shahrood, Iran.

Leake BE, Woolley AR, Arps CES, Birch WD, Gilbert MC, Grice JD, Hawthorne FC, Kato A, Kisch HJ, Krivovichev VG et al. (1997). Nomenclature of amphiboles: report of the subcommittee on amphiboles of the international mineralogical association, commission on new minerals and mineral names. Canad Mineral 35: 219-246.

Le Bas MJ (1962). The role of aluminum in igneous clinopyroxenes with relation to their parentage. Am J Sci 260: 267-288.

Leterrier J, Maury RC, Thonon P, Girard D, Marchal M (1982). Clinopyroxene composition as a method of identification of the magmatic affinities of Paleo-volcanic series. Earth Planet Sci Lett 59: 139-154.

Luhr JF, Carmichael ISE, Verekamp JC (1984). The 1982 eruptions of El Chichon volcano, Chiapas, Mexico: mineralogy and petrology of the anhydrite-bearing pumices. J Volcanol Geoth Res 23: 69-108.

MacKenzie WS, Smith JV (1955). The alkali feldspars: I. orthoclase-microperthites. Amer Miner 40: 707-732.

Molina J, Scarrow J, Montero PG, Bea F (2009). High-Ti amphibole as a petrogenetic indicator of magma chemistry: evidence for mildly alkalic-hybrid melts during evolution of Variscan basic–ultrabasic magmatism of Central Iberia. Contrib Mineral Petr 158: 69-98.

Moradi R, Boomeri M, Bagheri S (2014). Petrography and geochemistry of intrusive rocks in the Shurchah antimony-bearing area Southeast of Zahedan. Petrology (Isfahan University) 5: 15-32.

Müller D, Groves D (1997). Potassic Igneous Rocks and Associated Gold-Copper Mineralization. Berlin, Germany: Springer.

Nachit H (1986). Contribution a letude analytique et experimental des biotite des granitoids Applications typologiques. PhD, University of Western Brittany, Brest, France (in French).

Nachit H, Ibhi A, Abia EH, Ohoud MB (2005). Discrimination between primary magmatic biotites, re-equilibrated biotites and neoformed biotites. CR Geosci 337: 1415-1420.

Nakisa M (2002). Results of Exploration Studies and Reserves Estimation of the Lar Cu Ore Deposit-Zahedan. Tehran, Iran: Ministry of Industries and Mines, National Iranian Copper Industries Co.

Nimis P (1999). Clinopyroxene geobarometry of magmatic rocks. Part 2. Structural geobarometers for basic to acid, tholeiitic and mildly alkaline magmatic systems. Contrib Mineral Petr 135: 62-74.

Pang KN, Chung SL, Zarrinkoub MH, Khatib MM, Mohammadi SS, Chiu HY, Chu CH, Lee HY, Lo CH (2013). Eocene–Oligocene post-collisional magmatism in the Lut–Sistan region, eastern Iran: magma genesis and tectonic implications. Lithos 180-181: 234-251.

Panigrahi MK, Naik RK, Pandit D, Misra KC (2008). Reconstructing physico-chemical parameters of hydrothermal mineralization of copper at the Malanjkhand deposit, India, from mineral chemistry of biotite, chlorite and epidote. Geochem J 42: 443-460.

Patino Douce AE (1993). Titanium substitution in biotite: an empirical model with applications to thermometry, O_2 and H_2O barometers, and consequence for biotite stability. Chem Geol 108: 132-162.

Pirajno F (2010). Intracontinental strike-slip faults, associated magmatism, mineral systems and mantle dynamics: examples from NW China and Altay-Sayan (Siberia). J Geodyn 50: 325-346.

Rahnama-Rad J, Sahebzadeh B, Mirhajizadeh AA (2008). Weathering and weakness of Zahedan granitoids: a rock engineering point of view. Appl Geol 4: 247-257.

Ridolfi F, Renzulli A, Puerini M (2010). Stability and chemical equilibrium of amphibole in calc-alkaline magmas: an overview, new thermobarometric formulations and application to subduction-related volcanoes. Contrib Mineral Petr 160: 45-66.

Rieder M, Cavazzini G, D'Yakonov YS, Frank-Kamenetskii VA, Gottardi G, Guoggenheim S, Koval PV, Müller G, Neiva AMR, Radoslovich EW et al. (1998). Nomenclature of the micas. Canad Mineral 36: 905-912.

Saccani E, Delavari M, Beccaluva L, Amini S (2010). Petrological and geochemical constraints on the origin of the Nehbandan ophiolitic complex (eastern Iran): implication for the evolution of the Sistan Ocean. Lithos 117: 209-228.

Sadeghian M (2005). Magmatism, metallogeny and emplacement mechanisms of Zahedan granitoidic pluton. PhD, University of Tehran, Tehran, Iran.

Sadeghian M, Bouchez JL, Ne de lec A, Siqueira R, Valizadeh MV (2005). The granite pluton of Zahedan (southeast of Iran): a petrological and magnetic fabric study of a syntectonic sill emplaced in a transtensional setting. J Asian Earth Sci 25: 301-327.

Sadeghian M, Valizadeh MV (2007). Emplacement mechanism of Zahedan granitoidic pluton with the aid of AMS method. J Earth Sci 17: 126-143.

Sahebzadeh B (1996). Petrography and petrology of igneous intrusive of Zahedan-Lochan. MSc, Islamic Azad University, Tehran, Iran.

Siahcheshm K, Calagari AA, Abedini A, Lentz DR (2012). Halogen signatures of biotites from the Maher-Abad porphyry copper deposit, Iran: characterization of volatiles in syn- to post-magmatic hydrothermal fluids. Int Geol Rev 54: 1353-1368.

Sial AN, Ferreira VP, Fallick AE, Jeronimo M, Cruz M (1998). Amphibole rich clots in calc-alkalic granitoids in the Borborema province northeastern Brazil. J South Am Earth Sci 11: 457-471.

Soltanian A (2013). Petrogenesis of volcanic rocks from Lar complex, north of Zahedan, east of Iran. MSc, University of Sistan and Baluchestan, Zahedan, Iran.

Stöcklin J (1968). Structural history and tectonics of Iran, a review. Am Assoc Petrol Geol Bull 52: 1229-1258.

Tirrul R, Bell LR, Griffis RJ, Camp VE (1983). The Sistan Suture Zone of eastern Iran. Geol Soc Am Bull 94: 134-150.

Xianwu B, Ruizhong H, Hanley JJ, Mungall JE, Jiantang P, Linbo S, Kaixing W, Yan S, Hongli L, Xiaoyan H (2009). Crystallization conditions (T, P, fO_2) from mineral chemistry of Cu- and Au mineralized alkaline intrusions in the Red River-Jinshajing alkaline igneous belt, western Yunnan province, China. Mineral Petrol 96: 43-58.

Zarrinkoub MH, Pang KN, Chung SL, Khatib MM, Mohammadi SS, Chiu HY, Lee HY (2012). Zircon U–Pb age and geochemical constraints on the origin of the Birjand ophiolite, Sistan suture zone, eastern Iran. Lithos 154: 392-405.